P4.28 CLEAR SKY ANGULAR DEPENDENCE MODELS OVER OCEANS FROM CERES

Jianglong Zhang* and Sundar A. Christopher
University of Alabama in Huntsville, Huntsville, Alabama

Abstract

Measurements from the Earth Radiation Budget Experiment (ERBE) and the recent Clouds and the Earth's Radiant Energy System (CERES) have been successfully used in monitoring the outgoing energy from the earth-atmosphere system for more than three decades. These measurements include the broad band shortwave (SW) and longwave (LW) radiances at the top of the atmosphere, and angular distribution models (ADMs) are used to invert measured radiances to fluxes. Current ADMs, however, do not account for aerosols and surface effects such as wind speed. In this study, aerosol angular distribution models are constructed for biomass burning and dust regions for September 2000 over cloud free oceans, using the cross track and rotational azimuth plane scan mode CERES data. The Moderate-Resolution Imaging Spectroradiometer (MODIS) is collocated with CERES data, and used to discriminate aerosol scenes from totally clear and cloudy scenes within the CERES pixels. As indicated in this study, lack of dust aerosol ADMs could induce an increase in the derived SW aerosol direct forcing (SWARF) on the order of 20%. This study shows that at certain observation geometries, if ocean surface wind speeds are not considered when building ADMs, it could lead to maximum errors in shortwave fluxes on the order of 30-60%.

1. Introduction

In one of our previous papers [Christopher and Zhang, 2002], the Moderate-Resolution Imaging Spectroradiometer (MODIS) and Clouds and Earth's Radiant Energy System (CERES) data from Terra were used to study the aerosol SW forcing over clear oceans. The CERES was used to measure the changes in the top-of-atmosphere (TOA) short wave (SW) fluxes and the long wave (LW) fluxes with and without the presents of aerosols over cloud free oceans, and the MODIS cloud and aerosol products are used to identify cloudy, aerosol and clear CERES pixels. Several other studies have applied similar approaches to study the aerosol SW forcing [Christopher et al., 2000; Loeb and Kato, 2002]. The study of aerosol climate forcing is important because aerosols could counteract the global warming effect due to greenhouse gases [Hansen et al., 1998]. Unlike greenhouse gases, aerosols are poorly measured [Hansen et al., 1998], and remain one of the largest sources of uncertainty in climate change studies [IPCC 2001]. Traditional methods of addressing aerosol climate effects use either radiative transfer or general circulation models (GCMs) [e.g. Penner et al., 1992; Hansen et al., 1998]. However, characterizing the spatial and temporal distribution of aerosol physical and optical properties in models, remains a challenging problem. [e.g. Ramanathan et al., 2001, Barth et al., 2000, Tervahattu et al., 2002]. Using the combination of broadband and narrow band satellite measurements such as MODIS and CERES, we expect to minimize the level of details that are needed to obtain aerosol radiative forcing estimates. One of the advantages of using the MODIS/CERES combination is that the MODIS has a total of 36 channels and can detect aerosols and clouds with very high accuracy [Remer et al., 2002].

One of the major uncertainties associated with the aerosol SW forcing studies using MODIS and CERES is the angular distribution models (ADMs) [Christopher and Zhang, 2002; Wielicki et al., 1996]. The CERES does not measure the earth outgoing SW and LW fluxes directly. Therefore, the ADMs are used to relate the CERES measured radiances to fluxes at the given solar angle, satellite-viewing geometries, and surface and atmospheric conditions. The ADMs are represented by the anisotropic factor at each specific viewing geometry, and the anisotropic factor is the ratio between the assumed Lambertian flux to the real flux [Suttles et al., 1988]. For example, if the reflected or emitted energy is spatially uniform, the anisotropic factors will be 1 in all observing directions and the flux can be computed from the measured radiance by simply multiplying by a factor of π.

In our CERES/MODIS study [Christopher and Zhang, 2002], the CERES ES-8 data is used.

*Corresponding Author address: Jianglong Zhang, Department of Atmospheric Sciences, University of Alabama-Huntsville, Huntsville, AL 35806; zhang@nsstc.uah.edu.

The CERES ES-8 data set adopted the ERBE ADMs which are created for 4 different scene types over oceans: clear, partially cloudy, most cloudy and overcast [Suttles, 1988]. The effects of ocean winds and aerosols are not explicitly included in the ERBE ADMs. Theoretical calculation showed that the upward radiance at the top-of-atmospheric could behave differently when ocean-surface wind speed and direction changes [e.g. Masuda, 1998]. Li et al., [2000] showed that aerosols, which are inhomogeneously distributed spatially, could absorb and scatter the SW radiation, and change the angular distribution pattern of the TOA outgoing SW energy. Therefore the effects of both wind speed and aerosols to the CERES Ocean SW ADMs must be studied.

2. Data

The CERES ES-8 data, which uses the ERBE ADMs, provides top of atmosphere (TOA) SW (0.3-5 μm) radiances and fluxes. The CERES instrument on Terra operates in three modes; the cross-track scan mode that is similar to the ERBE, the along-track scan mode that is used in validation of instantaneous fluxes and the rotating azimuth plane scan mode that is used in building ADMs [Wielicki, et al., 1996]. In this study, both the cross-track and rotational azimuth plane scan mode data are used.

The CERES on Terra has a large footprint on the order of ~30 km at nadir [Wielicki et al., 1996]. Therefore, it is difficult to separate CERES pixels into either totally clear, aerosol or cloudy using CERES observations alone. On the contrary, MODIS, which is on the same satellite platform as CERES, has a much finer resolution on the order of 250 m to 1000 m [Kaufman et al., 1997]. Therefore, the MODIS can be used to provide aerosol optical properties (MOD04) and cloud fraction (MOD06) information within the CERES footprints. The MODIS level-2 aerosol product (MOD04) provides retrieved aerosol optical thickness (0.55μm) and other aerosol properties at 10 km spatial resolution. Based on theoretical sensitivity studies using radiative transfer algorithms, the uncertainties in AOT retrievals are estimated to be ± 0.05± 0.20 AOT over land [Kaufman et al., 1997] and ± 0.05± 0.05 AOT over ocean [Tanré et al., 1997]. The MODIS level 2 cloud product (MOD06) provides cloud screened data at both 1 and 5 km resolution [King et al., 1992; Ackerman et al., 1998]. Due to the computational expense, only 5 km resolution MOD06 data is used.

The wind speeds are obtained from the Special Sensor Microwave Imager (SSM/I) daily product. and is well calibrated using more than 72,000 buoy and radiosonde observations[Wentz, 1997]. A recent study showed that the mean and the standard deviation of the difference between SSM/I and buoy wind speeds are less than 0.4m/s and 1.4m/s respectively for SSM/I data [Mears et al., 2001].

3. Method

In the first step, MODIS and CERES data are collocated [Christopher and Zhang, 2002] to screen out cloud-contaminated sky CERES pixels. Only CERES pixels that have cloud fraction less than 5% (from MOD06) are used in the analysis. For a CERES pixel that does not have valid MODIS AOT retrievals within the footprint, the nearest MODIS AOT retrieval is used. The CERES pixels with cloud fraction larger than 0% but less than 5% are used to increase number of data samples. The cloud and aerosol free (AOT less than 0.02) CERES pixels are further divided into 4 groups of data with wind speed ranges of 0-3, 3-6, 6-9, 9-12 m/s respectively, based on the SSM/I wind product.

During CERES observations, the unfiltered radiances are first determined from the measured filtered SW (0.2-5.0μm) and LW (5.0-50μm) radiances. The unfiltered radiances are then converted into SW and LW fluxes using the ADMs that relate radiance to flux at given observing conditions as shown in equation 1 and 2 [Suttles et al., 1988].

$$M(q_0) = \int_{f=0}^{2p} df \int_{q=0}^{2p} dq L(q_0, q, f) \cos q \sin q \qquad (1)$$

$$M(q_o) = pL(q_o, q, j) / R(q_o, q, j) \qquad (2)$$

Where M is flux, L is the measured unfiltered radiance and R is the anisotropic factor. θ_o, θ, φ are the solar zenith angle (SZA), satellite viewing zenith angle (VZA), and azimuth angle (AZM) respectively.

In this study, the radiation field is separated into finite angular bins (7 viewing zenith angles and 8 azimuth angles) as described in Suttles et al [1988]. Since solar zenith angles (at the satellite observation time) do not vary significantly in one month for a given region, the

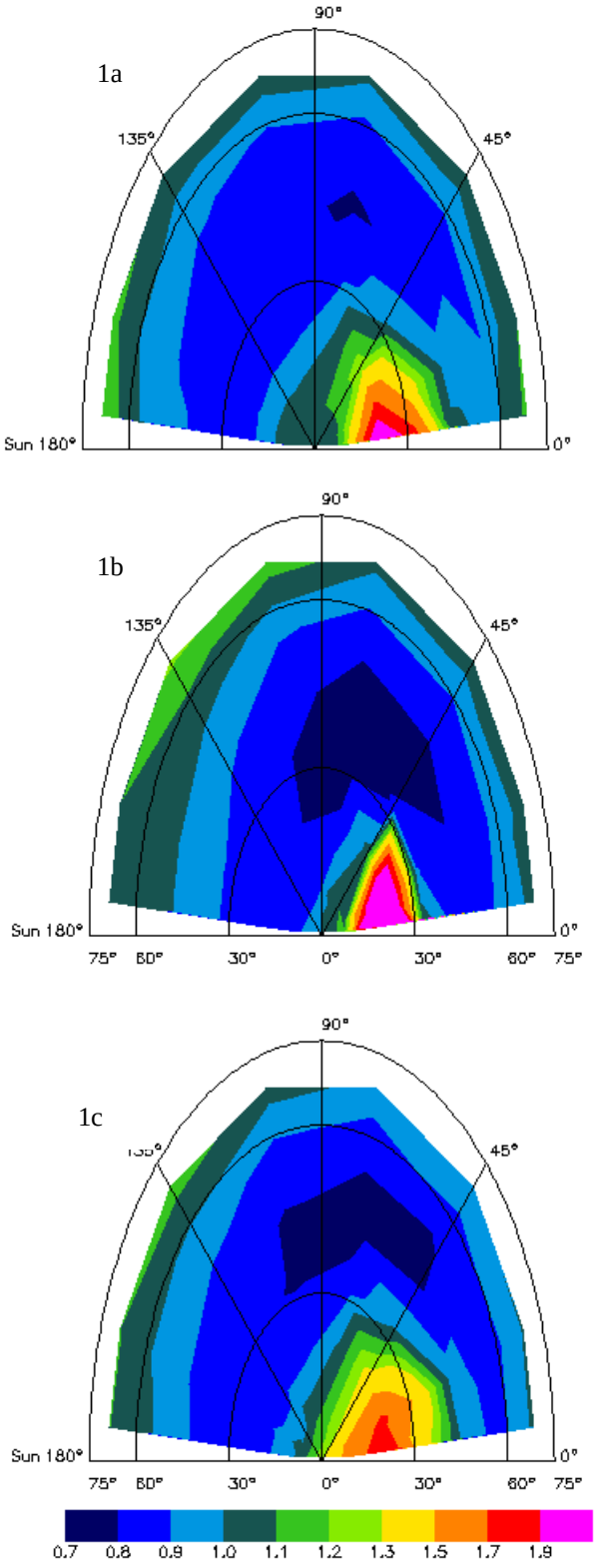

Figure 1. Polar plots for the SW clear-sky ADMs at the 0°-25° SZA bin. Radii represent the VZAs and polar angles represent the AZMs. Sun is located at the 180° AZM. a). Polar plot of the ERBE clear-sky SW ocean ADM. b) Polar plot of the low wind (0-3 m/s) clear-sky ocean ADM. c) Polar plot of the high wind (9-12 m/s) clear-sky ocean ADM.

solar zenith bins are chosen selectively instead of using the full spectrum of solar zenith angle bins. Therefore, for a given range of SZA and given ranges of wind speed and AOT, the equation (1) can be rewritten as [Suttles et al., 1988].

$$M_i = \sum_{k=1}^{8} (f_{k+1} - f_k) \sum_{j=1}^{7} \bar{L}_{ijk} (\sin^2 q_{j+1} - \sin^2 q_j) \qquad (3)$$

Where the variables i, j and k in equation (3) are the indices for solar zenith, viewing zenith, and azimuth angle bins respectively.

Over cloud and aerosol free ocean scenes, ADMs are built by binning CERES unfiltered radiances as a function of wind speed, solar angle, and satellite viewing angles. In this study, the clear-sky SW Ocean ADMS are built for two solar zenith angle bins of 0°-25° and 25°-36°, and for wind speed ranges of 0-3, 3-6, 6-9 and 9-12 m/s. Only CERES pixels that have collocated AOT values less than 0.05 are used.

The aerosol ADMs are also built for three selected regions for AOT range of 0.05-0.25 and 0.25-0.5, where large SWARF values are reported for September 2000 [Christopher and Zhang, 2002; Zhang and Christopher, 2003, this issue]. The three regions are: (1) South Africa (SA) (0-40°S, 30-50°E), (2) Australia (AUS) (0-20°S, 110-130°E), (3) North Africa (NAF) (10-30°N, 10-40°W). The aerosol ADM are built for three SZA bins 0°-25°, 25°-36° and 36°-45° for the SA region, and are built for two SZA bins 0°-25°, 25°-36° for the AUS and NAF regions.

4. Results and discussion

4.1 Clear Sky Ocean Wind ADMs

Figure 1a shows the polar plot of the ERBE SW clear-sky ocean ADM for the SZA bin of 0°-25°. The radius of the polar plot represents the viewing zenith angle, and the polar angle represents the azimuth angle. The sun is located at 180° AZM. The center of the polar plot is at the satellite nadir view (0° VZA, 0° AZM). The strong-sunglint regions, which is defined to be the regions that have SW anisotropic factors greater than 1.9 in this study, are shown in pink and are located between 15°-28° VZA and 0°-20° AZM. The sub-sunglint regions, which are the regions surrounding the strong-sunglint regions with anisotropic factors greater than 1.1 but less than 1.9, are between 10°-45° VZA and 0°-50° AZM. Figure 1b shows the clear-sky SW low wind speed (0-3m/s) ADM for the same SZA bin as Figure 1a. The specular reflectance is larger in Figure 1b when compared to Figure 1a. The sub-sunglint

regions in Figure 1b, however, cover much narrower regions within the areas from 10°-30°

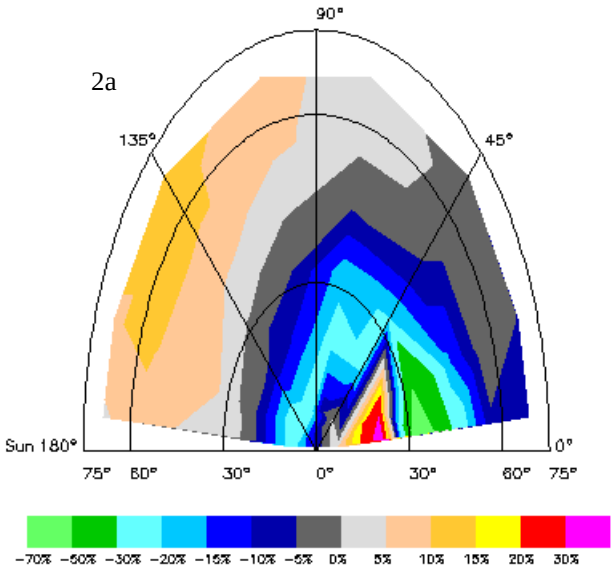

Figure 2. Polar plots for the relative uncertainties of the retrieved CERES ES-8 SW fluxes at the 0°-25° SZA bin. Radii represent the VZAs and polar angles represent the AZMs. Sun is located at the 180° AZM. a). Relative uncertainties of the retrieved CERES ES-8 fluxes over regions with the low speed (0-3 m/s) near surface wind. b) Relative uncertainties of the retrieved CERES ES-8 fluxes over regions with the high speed (9-12 m/s) near surface wind

VZA, and 0°-45° AZM. Figure 1c shows the clear-sky SW ocean ADM for wind speeds from 9 to 12 m/s. The angular distribution pattern for the high wind clear-sky ocean are similar to that of the ERBE clear ocean SW ADM.

The changes in anisotropic factors in the strong-sunglint and sub-subglint regions as a function of wind speed can be explained by the interactions between wind and ocean surfaces. For calm oceans, when the wind speeds are less than 3m/s, the ocean surfaces are relatively flat and the sun light is specularly reflected. The sunglint effects decrease dramatically as the viewing geometries changes. At higher wind speeds, the ocean surfaces act as diffuse reflectors and whitecaps are formed [Cox and Munk, 1954a; b]. Thus, in the strong-sunglint regions, sunlight that was supposed to be specularly reflected has been scattered in all directions because ocean surfaces no longer reflect like flat mirrors. Therefore, the reflectance in the strong-sunglint regions is weakened.

By differentiating equation (2) we can obtain the following equation:

$$\Delta M/M = -\Delta R(\theta o,\theta,\varphi)/R(\theta o,\theta,\varphi) \qquad (4)$$

Equation (4) indicates that the relative uncertainty of the inverted flux is proportional to the uncertainty of the anisotropic factor and is inversely proportional to the anisotropic factor at a given solar and viewing angles. Figure 2a shows the relative uncertainties of fluxes (as defined in equation 4) retrieved at the 0-3 m/s wind speed range using the ERBE clear-sky SW ocean ADM at 0°-25° SZA. The largest overestimation is in the strong-sunglint region with maximum uncertainties of above 30% implying that the anisotropic factors from the low wind ADM are much larger than that of the ERBE clear-sky SW Ocean ADM at the sunglint regions. At the back scattering regions where VZA is greater than 30°, the ERBE clear-sky SW ocean ADM overestimates the fluxes by about 5-15%. Figure 2b shows the uncertainties of using ERBE ADM at high wind (9-12 m/s) speeds. For the majority of the angles, the uncertainties are less than 5%. The largest overestimates are found to be 20-30% in the sunglint regions and the largest underestimates of 20-30% are found at 0° AZM and 32° VZA.

We further test the case when observations from all angular bins are included. If we assume the CERES observations are equally distributed in all the angular bins, the uncertainties of the ERBE ADMs due to lack of the wind speed factor can be estimated by averaging the estimated relative uncertainties based on equation (4). The estimated uncertainties are 5%, 3%, 1% and 1% for data observed at the wind speed

ranges of 0-3, 3-6, 6-9 and 9-12 m/s respectively for the SZA bin of 0°-25°, and are 3%, 2%, 1% and 0% for the SZA bin of 25°-36°.

4.2 Aerosol ADM

Figure 3a shows the MODIS AOT vs. CERES SW flux for the three different regions: (1) South Africa, (2) Australia, (3) North Africa. To be consistent with our previous studies [Zhang and Christopher, 2003, this issue; Christopher and Zhang, 2002], sunglint regions are excluded from the study, and only the CERES pixels that have valid collocated are used.

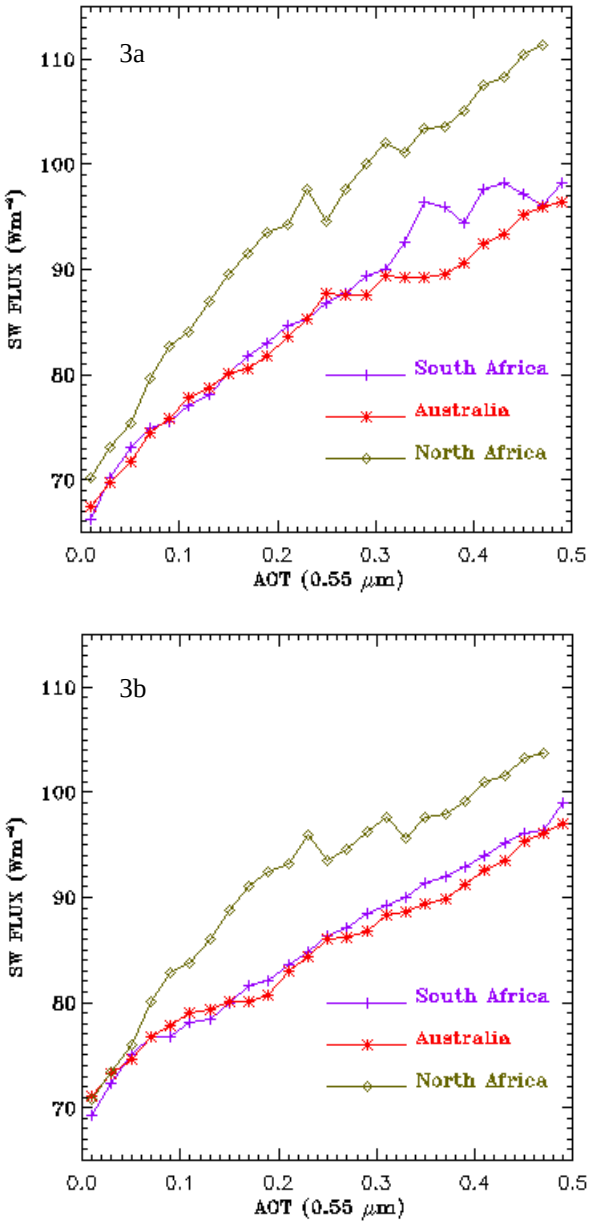

Figure 3. a) MODIS AOT vs. CERES flux for three different regions: South Africa, Australia, and North Africa. b). Similar as figure 3a, except the new aerosol ADMs are used to invert radiances to fluxes.

The SA and AUS regions have similar aerosol forcing values, while the NAF region has a higher SWARF/AOT value. The dominant aerosol types for SA and AUS regions are biomass-burning aerosols, while the dominant aerosol type in the NAF region is dust. Figure 3b is similar to figure 3a except that the new aerosols ADMs are used instead of the ERBE ADMs. Figure 3b shows that for the AUS and SA regions, where smoke aerosols are prevalent, the changes in the SWARF due to ADMs are small and are within the uncertainties in this study. For the NAF region, dominated by dust aerosols, the differences in the SWARF due to ADM's are on the order of 20% for the AOT range of 0.25 to 0.5. Therefore, as suggested in this study, aerosol ADMs are needed for dust regions. The uncertainties in the aerosol and ocean wind speed ADMs could arise from four main sources including cloud contamination, ocean winds, the uncertainties in MODIS aerosol retrievals, and interpolation errors.

5. Conclusions

The focus of this paper is to study the wind and aerosol effects on the ERBE clear-sky SW Ocean ADMs. The careful categorization of the clear-sky SW Ocean ADMs is important because it is one of the critical steps needed to reduce the uncertainties in aerosol forcing studies using CERES observations. This study shows that the wind speed is an important factor that needs to be included in CERES ocean ADMs. If wind speeds are not included this could cause maximum uncertainties of 30-60% at sunglint and sub-sunglint angles. This study also showed that on the average, at low aerosol optical thickness ranges (0.25 -0.5), lack of dust ADMs could induce a 20% increase in the estimated SWARF over dust regions. However for areas with smoke aerosols, the uncertainties due to a lack of smoke ADMs are negligible.

Acknowledgements. This was supported by NASA's ESS fellowship and NASA's Global Aerosol Climatology Project (GACP). The CERES data were obtained from the NASA Langley Research Center Atmospheric Sciences Data Center and the MODIS data were obtained through the Goddard Space Flight Center Data Center. We also thank the CERES science team

for providing the CERES point spread function and geolocation information.

References

Ackerman, S. K. Strabala, P.Menzel, R. Frey, C. Moeller, and L. Gumley, Discriminating clear sky from clouds with MODIS. J. Geophys. Res., 103, 32,141-32,157, 1998.

Barth, M. C., P. J. Rasch, J. T. Kiehl, C. M. Benkovitz, and S. E. Schwartz, Sulfate chemistry in the National Center for Atmospheric Research Community Climate Model: Description, evaluation, features, and sensitivity to aqueous chemistry, *J. Geophys. Res.,* 105, 1387-1415, 2000.

Christopher, S. A., and J. Zhang, 2002: Shortwave aerosol radiative forcing from MODIS and CERES observations over the oceans. *Geophys. Res. Letters*, In press, 2002. (http://vortex.nsstc.uah.edu/~sundar/papers/grl_2002.pdf)

----------, J. Chou, J. Zhang, X. Li and R.M. Welch, Shortwave Direct Radiative Forcing of Biomass Burning Aerosols Estimated From VIRS and CERES. *Geophys. Res. Letters, 27*,2197-2200, 2000a.

Cox, C., and Munk, W., Measurements of the roughness of the sea surface from photographs of the sun's glitter, *J. Opt. Soc. Am*. 44, 838-850, 1954a.

Cox, C., and Munk, W., statistics of the sea surface derived from sun glitter, *J. Mar. Res*, 13, 198-227, 1954b.

Hansen, J., M. Sato, A. Lacis, R. Ruedy, I. Tegen, and E. Matthews, Climate forcings in the Industrial era, *Proc. Natl. Acad. Sci., 95*, 12753-12758, 1998.

Harrison, E. F., P. Minnis, B. R. Barkstrom, V. Ramanathan, R. D., Cess, and G. G. Gibson, Seasonal variation of cloud radiative forcing derived from the Earth Radiation Budget Experiment, *J. Geophys. Res.,* 95, 18,678-18,703, 1990.

Kaufman, Y. J., D. Tanré, L.A. Remer, E. Vermote, A. Chu and B.N. Holben, Operational remote sensing of tropospheric aerosol over land from EOS moderate resolution imaging spectradiometer., *J. Geophys. Res*., *102,* 17051-17067, 1997.

King, M. D., Y. J. Kaufman, W. P. Menzel, and D. Tanre, Remote Sensing of Cloud, Aerosol, and Water Vapor Properties from the Moderate Resolution Imaging Spectrometer (MODIS), *IEEE Trans. Geo. Rem. Sens., 30*, 2-27, 1992.

Li, X., S.A. Christopher, J. Chou, and R.M. Welch, Estimation of shortwave direct radiative forcing of biomass burning aerosols using angular dependence models. J. Appl. Meteor., 39, 2278-2291, 2000.

Loeb, N. G., and S. Kato, Top-of-Atmosphere direct radiative effect of aerosols from the Clouds and the Earth's Radiant Energy System Satellite instrument (CERES), *J. Climate*,*–, 15*, 1474-1484, 2002.

Masuda, K., Effects of the speed and direction of surface winds on the radiation in the atmosphere-ocean system, *Remote Sens. Environ*, 64, 53-63, 1998.

Mears, C., D. Smith, and F. J. Wentz, Comparison of SSM/I and buoy-measured wind speeds from 1987 - 1997, *J. Geophys. Res.*, 106, 11,719-11,729, 2001.

Ramanathan, V., and coauthors, Indian Ocean Experiment: An integrated analysis of the climate forcing and effects of the great Indo-Asian Haze, *J. Geophys. Res.*, 106, 28,371-28,398, 2001.

Remer, L. A., Y. J. Kaufman, Z. Levin and S. Ghan, Model assessment of the ability of MODIS to measure top of atmosphere direct radiative forcing from smoke aerosols. *J. Atmos. Sci*. GACP special issue (in press), 2002.

Penner, J. E., R. E. Dickinson, and C. A. O'Neill, Effects of aerosol from biomass burning on the global radiation budget, *Science*, *256*, 1432-1434, 1992.

Suttles, J. T., and Coauthoes, Anglular radiation models for earth-atmosphere system. I - Shortwave radiation, *NASA RP-1184*, 144pp, 1988.

Tanré, D., Y.J. Kaufman, M. Herman and S. Mattoo, Remote sensing of aerosol properties over oceans using the MODIS/EOS spectral radiances., *J. Geophys. Res., 102*, 16971-16988, 1997.

Tervahattu, H., K. Hartonen, V.-M. Kerminen, K. Kupiainen, P. Aarnio, T. Koskentalo, A. F. Tuck, and V. Vaida, New evidence of an organic layer on marine aerosols, *J. Geophys. Res.*, 107(D7), 2002.

Wentz, F.J., A well-calibrated ocean algorithm for Special Sensor Microwave/Imager, *J. Geophys. Res.,* 102 (C4), pp8703-8718, 1997.

Wielicki, B. A., B. R. Barkstrom, E. F. Harrison, R. B. Lee III, G. L. Smith, and J. E. Cooper, "Clouds and the Earth's Radiant Energy System (CERES): An Earth Observing System Experiment," *Bull. Amer. Meteor. Soc.*, *77*, 853-868, 1996.

Zhang, J. and S. A. Christopher, Short wave aerosol direct forcing over cloud free oceans from Terra, this issue, 2003.